

Unsteady Aerodynamic Computations Using Dual-Time-Step Technique

Hugo Stefano de Almeida, almeida_hsa@yahoo.com.br

Instituto Tecnológico de Aeronáutica - ITA - Brasil

João Luiz F. Azevedo, joaoluiz.azevedo@gmail.com

Instituto de Aeronáutica e Espaço - CTA/IAE/ALA - Brasil

Abstract. *The present effort has the objective to predict the unsteady aerodynamic responses of some airfoils in terms of the aerodynamic delay. The airfoil response is obtained by means of the unsteady flow delay. The aerodynamic delay represents, how fast the flow field response is, with respect to the airfoil movement. Typically, this response is viewed by the hysteresis curves. These curves computes the aerodynamic coefficients, as a function of the airfoil, degrees of freedom (DOFs) motion. Unsteady simulations are performed at transonic Mach numbers in order to capture main effects of inviscid formulation. In this regime of flow, the most common linear aeroelastic analysis, based on the a linear aerodynamic theory, present poor results in comparison with experimental data. Hence, this is the motivation to using CFD techniques to predict aerodynamic coefficients distributions at each time step. A Dual-time-Step algorithm performance is also evaluated in this effort, and some convergence accelerating techniques are also implemented in aeroelastic solver to increase convergence ratio. The 2-Dimensional, 2-D, compressible, unsteady Euler equations, in the dimensionless form, represent one of useful models for the flows of interest. For the proposes of the present work, this model well captures flow field phenomena of interest. The solver is written in a finite volume method context, hence the Euler equations are solved integrating by volume over the domain control volumes. A centred spatial discretization scheme with explicit artificial dissipation is used. A mesh movement algorithm is used in order to provide unsteady aerodynamic results compatible with mesh movement requirements. Mesh movement algorithm simulate a forced harmonic motion imposed to the airfoil in a certain frequency, known a priori. This is the reduced frequency of the airfoil. Moreover, some viscous flows are computed in steady flow field condition. Results are compared with inviscid formulation. Viscous formulation is implemented by means of Spalart-Allmaras turbulence model. The viscous terms validation is required to solve unsteady formulation using viscous formulation.*

Keywords: CFD, Dual-Time-Step, Unsteady Aerodynamics

1. INTRODUCTION

Over the past few years, the Computational Aerodynamics Laboratory of Instituto de Aeronáutica e Espaço (IAE) has been developing CFD solvers for two and three-dimensional steady inviscid and viscous flows (see Strauss and Azevedo, 1999, Bigarella and Azevedo, 2007). Since the last decade the research group, have been working with unsteady and non-viscous flows for transonic aerodynamic problems (see, for instance, Oliveira, 1993). Afterwards, Simões and Azevedo(1999) has simulated the same transonic cases. An analysis of mesh dependency for steady and unsteady results was the main objective of that work. Better results are obtained for steady and unsteady cases, provided that a sufficiently refined mesh is used and, still, one observes a large dependency of mesh refinement in the final results, specially for aerodynamic coefficient computations. Recently, Marques(2004) reviewed the work of Oliveira with more detailed information, and extended the analysis for flat plate cases. In his work results are compared with Theodorsen analytical theory. The present work intends to complement Marques' work, comparing his inviscid results with those from viscous turbulent solvers and extend the applications to supercritical profiles in which mesh and viscous dependency, even for steady results, is expected to be larger than for conventional profiles.

It is known that inviscid solvers can provide good results to steady flows over conventional airfoils flying at transonic Mach numbers, as indicated in Lisandrin, et al.(2006) and Hsu, et al.(2002). The unsteady results obtained by the same authors compare well with experimental data for some aerodynamic coefficients. However, simulations of previously referred authors used conventional airfoils. Moreover, although lift coefficient results were in agreement with the available experimental data, the moment coefficient, C_m , presented poor results, as shown, for instance, in Marques(2004) and Raush et al.(1990). Recently, Raveh(2008) and Darracq et al.(1998), obtained good results for unsteady transonic cases with large shock-wave oscillations for some conventional airfoils too. They compared results obtained with different turbulence models and results agree very well with experimental data. It is noteworthy that even the moment coefficient, which is more sensitive to viscous structures than the force coefficients, is in good agreement with the comparison data.

A Dual-Time-Step technique was implemented in solver to increase capability to well predict aerodynamic coefficients distribution on airfoil surface. Better results is expected in even using inviscid formulation. A set of inner iterations is expected for each real time step, as will be seen in few sections. Hence, better convergence is expected to be achieved using this formulation. Using a dual-time stepping scheme some changes may be implemented in multigrid scheme. This scheme shall be able to predict unsteadiness conditions of flow field and transport information through other multigrid mesh levels. This scheme is used to increase convergence ratio in unsteady flows (see Jameson, 1991).

The 2-D steady and unsteady Reynolds-averaged Navier-Stokes (URANS) equations are the formulations implemented in the CFD solver. This code is written in a cell centred finite volume context for unstructured meshes. The solver is able to handle any type of mesh, since it is built using a face-based (actually, edge-based in 2-D) data structure, in which properties are computed at faces and the contribution to shared volumes is distributed accordingly. A modified explicit time marching scheme, based on the well-known 5th-order Runge-Kutta scheme, is used to advance the solution in time. This scheme is written to support steady and unsteady simulations. In the latter case, one must also provide support for the contribution of mesh deformation. Moreover, an implicit Euler method is used to solve the turbulence model equations, as previous experience of Bigarella and Azevedo(2007) indicated that an implicit time integration is required to maintain numerical stability of turbulence models. Further, the convective terms of the Spalart and Allmaras(1994) turbulence model are discretized on a 1st-order upwind flux scheme. This task is used to avoid adding explicit artificial dissipation terms to maintain stability of the solution. All other terms of the governing equations are spatially discretized using the equivalent of a central spatial discretization scheme plus added artificial dissipation Jameson et al.(1981) and Jameson and Mavriplis(1986).

2. AERODYNAMIC FORMULATION

The problems of interest in the present work can be adequately represented by the 2-D Euler and/or Navier-Stokes equations. The 2-D URANS equations can be written in dimensionless and conserved form as

$$\frac{\partial Q}{\partial t} + \frac{\partial E}{\partial x} + \frac{\partial F}{\partial y} = 0. \quad (1)$$

where E and F are fluxes vectors from URANS set of equations which contain contribution of inviscid and viscous terms. These flux vectors can be written as

$$\begin{aligned} E &= E_e - E_v, \\ F &= F_e - F_v. \end{aligned} \quad (2)$$

The vector of conserved variables and the convective flux vectors are

$$Q = \begin{Bmatrix} \rho \\ \rho u \\ \rho v \\ e_i \end{Bmatrix}, \quad E_e = \begin{Bmatrix} \rho U \\ \rho u U + p \\ \rho v U \\ (e + p)U + x_t p \end{Bmatrix}, \quad F_e = \begin{Bmatrix} \rho V \\ \rho u V \\ \rho v V + p \\ (e + p)V + y_t p \end{Bmatrix}. \quad (3)$$

The subscript “e” indicate Euler fluxes on vector terms. The contravariant velocity components, U and V , carry, for unsteady cases, the contributions from mesh velocities. The present approach initially computes the node mesh velocity components. However, since the code uses a cell centred method, such node velocity components are averaged in order to yield volume centroid velocity components, x_t and y_t . Hence, U and V can be written as

$$U = u - x_t, \quad V = v - y_t. \quad (4)$$

The viscous flux vectors, E_v and F_v , are given by a linear composition of stress tensor terms, τ_{ij} , and heat transfer vector, q . Hence, one can write

$$E_v = \frac{M_\infty}{Rey} \begin{Bmatrix} 0 \\ \tau_{xx} \\ \tau_{xy} \\ \tau_{xx}u + \tau_{xy}v - q_x \end{Bmatrix}, \quad F_v = \frac{M_\infty}{Rey} \begin{Bmatrix} 0 \\ \tau_{xy} \\ \tau_{yy} \\ \tau_{xy}u + \tau_{yy}v - q_y \end{Bmatrix}. \quad (5)$$

The Reynolds number, Rey , appears in the previous expressions from the dimensionless URANS equation procedure, as well he Mach number, M_∞ . In the present work, the Reynolds and Mach numbers are computed in reference to the airfoil chord, c , and the free stream velocity magnitude as

$$Rey = \frac{\rho_\infty q_\infty c}{\mu_\infty}, \quad M_\infty = \frac{q_\infty}{a}, \quad (6)$$

where, a is the speed of sound. The q_∞ variable is the velocity magnitude in the free stream. For a 2-D code, it is defined as $\sqrt{u_\infty^2 + v_\infty^2}$. The problem requires some constitutive relations in order to have equal number of equations and the number of flow field variables. Hence, pressure is computed by the equation of state for perfect gases as

$$p = (\gamma - 1) \left[e_i - \frac{1}{2} \rho (u^2 + v^2) \right]. \quad (7)$$

In the previous equation, γ is the ratio of specific heats, and it taken as 1.40 for all calculations here performed, as usual for air. The viscous stress tensor and the heat flux vector, written in Einstein's indicial form, are given by

$$\tau_{ij} = (\mu_l + \mu_t) \left[\left(\frac{\partial u_i}{\partial x_j} + \frac{\partial u_j}{\partial x_i} \right) - \frac{2}{3} \frac{\partial u_n}{\partial x_n} \delta_{ij} \right], \quad q_j = -\gamma \left(\frac{\mu_l}{Pr} + \frac{\mu_t}{Pr_t} \right) \left(\frac{\partial e_i}{\partial x_j} \right). \quad (8)$$

Usually in URANS codes, the contribution from small turbulence scales of time, space, and vorticity are added explicit into the flux vector and stress tensor. As can be seen in Eq. 8, this contribution is formed by adding the so-called turbulent viscosity coefficient, μ_t . This variable assumes a zero value in freestream regions, once no turbulence is generated, to higher values near specific regions of the domain, usually near walls, in boundary layers, and in the airfoil wake in aerodynamic problems.

The turbulence model Spalart-Allmaras(1994), is used in the present viscous simulations by modelling the scales of turbulent flow. This is a robustness model which requires less refined meshes near wall regions, $y^+ = 1$. This model is very used in aerodynamic applications and fully description of the model can be viewed in Spalart-Allmaras(1994).

3. DUAL-TIME-STEP TECHNIQUE

A dual time step algorithm was implemented in the aeroelastic solver. This technique is implemented to solve an instability problem of unsteady viscous simulations, mainly. Motivation using this technique concern about increasing time steps, or time scales, of unsteady flows without loss of accuracy of numerical data. These are usually small enough to invalidate unsteady simulation in terms of real time steps usage. Steady simulations performed so far, requires small time steps.

A dual-time-step algorithm technique was implemented in accordance to Jameson(1991). The objective of using this technique is solving for each real time step a steady simulation in pseudo-time, which convergence criterion shall be met or maximum number of iterations Jameson(1991) and Hsu and Jameson(2002). Usually, maximum number of iterations is son met than convergence criterion. Chart flow graphic in Fig. 1 shows how dual-time-step technique was implemented in solver.

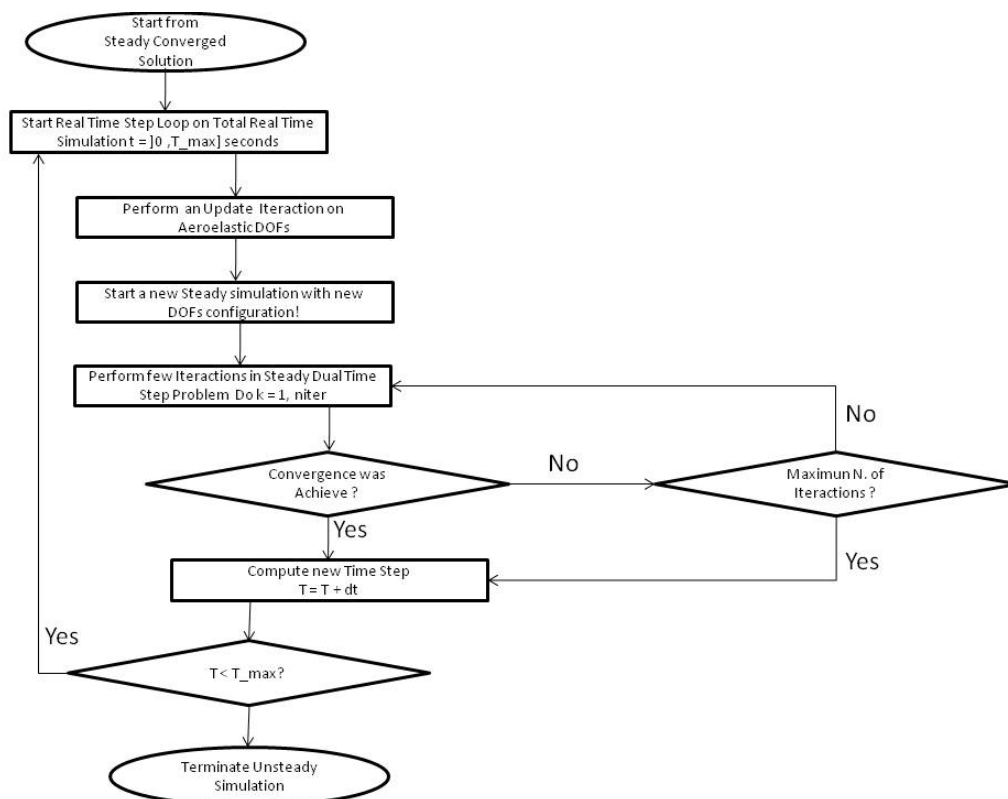


Figure 1. Chart Flow of Dual-Time-Step Algorithm.

Implementation of this technique lead to solving a steady simulation for each update in aeroelastic DOFs. Furthermore, all acceleration convergence techniques are used in order to faster achieve convergence in pseudo-time. There are two

time steps used in a full unsteady dual-time-simulation: 1) first one, the real time, perform update of aeroelastic DOFs, and 2) a pseudo time-step used to converge simulation in few inner iterations of steady problem.

First of all, the solver reads initial data from a steady converged simulation. In a second stage, pseudo-time step iterations are performed using all convergence acceleration techniques at hands. Convergence criteria are performed for both convergence and maximum number of inner iterations at each steady simulation in pseudo-time. Finally, as a convergence criteria is match, an airfoil update is performed considering current solution, and source term of unsteady multigrid algorithm is computed. It is constant along inner iterations in current time step, and shall be zero at first two iterations in order to maintain convergence of method. After all, the cycle is restarted for a new steady simulation for a new time step.

4. SPATIAL DISCRETIZATION

The CFD solver used in the present work was largely used and validated in inviscid and viscous simulations (see for instance Marques, 2007 and Strauss, 1999, respectively). This solver was build in a centered finite volume context. The finite volume method performs an integration of Eq. 1 in each control volume of the flowfield. After integration and posterior application of Green's theorem, one obtain

$$\frac{\partial}{\partial t} \int_{\mathcal{V}} Q d\mathcal{V} + \int_S (E dy - F dx) = 0. \quad (9)$$

The discrete vector of conserved variables for the $i - th$ control volume, Q_i , is defined as

$$Q_i = \frac{1}{\mathcal{V}_i} \int_{\mathcal{V}_i} Q d\mathcal{V}. \quad (10)$$

Now, the problem is how to obtain the flux throughout the faces of each control volume of the discrete domain. Mavriplis(1990), suggested that the flux computation at each face must carry some information, flow field variables, of the neighbouring volumes which share this face. The flux computations at the face, is given by

$$\int_{s_i} (E dy - F dx) \approx \widehat{C}(Q_i) = \sum_{k=1}^{s_i} [E(Q_k)(y_2 - y_1) - F(Q_k)(x_2 - x_1)]. \quad (11)$$

Flux contributions $E(Q_k)$ and $F(Q_k)$ are computed with the prescribed value in the face, Q_k , so this contribution is added to $i - th$ volume and subtracted from its neighbour, $nb - th$ control volume. Furthermore, any property which needs to be measured at the face, must be estimated as a simple average between the adjacent volumes, i and nb , which share the $k - th$ face. For a general variable at the $k - th$ face, one can write

$$\psi_k = \frac{\psi_i + \psi_{nb}}{2}, \quad (12)$$

where, ψ is a generic variable. The viscous flux derivatives are also compute by a surface integration over control volume faces, according to Swanson(1991). High order spatial discretization schemes are beyond the scope of this work.

Some artificial dissipation is required in order to maintain the numerical stability of the simulation. Once a centered spatial discretization scheme is used, explicit addition of artificial dissipation is required because a centered scheme is, by construction, undamped, and, therefore, it allows the generation of numerical instabilities. Those instabilities appear, mainly, as oscillations in regions of strong gradients, such as in shock wave regions. Mavriplis(1990) has proposed the following artificial dissipation scheme

$$\widehat{D}(Q_i) = \xi_{i,nb}^2 d^2(Q_i) - \xi_{i,nb}^4 d^4(Q_i). \quad (13)$$

The d^2 and d^4 operators are, respectively, the undivided Laplacian and biharmonic operators. The first term is related to damping numerical instabilities in the presence of shock waves and the second term is responsible for the background stability. Further details about artificial dissipation operators can be viewed in Mavriplis(1990).

5. TEMPORAL DISCRETIZATION

The temporal scheme used emerged from the 5th-order, 5th-stage, explicit Runge-Kutta(RK5) time advancing scheme. However, in order to guarantee a higher robustness to a large range of applications, which is achieved by increasing the linear stability limit at the expense of accepting a lower order of accuracy, Jameson et al.(1981) proposed some new α coefficients. In order to take into account the unsteady flow phenomena, Batina(1991) proposed some changes on Jameson's work. Batina proposal concerns the addition of the contribution of the ratio of control volume deformation. This contribution is felt in terms of induced edge velocities and volume variation. This volume variation is explicitly taken

into account into the RK5 scheme as a ratio between the value of the $i - th$ control volume area in two consecutive time steps.

$$\begin{aligned} Q_i^{(0)} &= Q_i^n, \\ Q_i^{(j)} &= \frac{\nabla_i^n}{\nabla_i^{n+1}} Q_i^{(0)} - \alpha_j \frac{\Delta t_i}{\nabla_i^{n+1}} \left[\widehat{C} \left(Q_i^{(j-1)} \right) - \widehat{D} \left(Q_i^{(j-1)} \right) - \widehat{V} \left(Q_i^{(0)} \right) \right], \\ Q_i^{n+1} &= \frac{\nabla_i^n}{\nabla_i^{n+1}} Q_i^{(5)}. \end{aligned} \quad (14)$$

The residue operator, RHS , computed for $i - th$ control volume, is composed by the summation of convective terms, the artificial dissipation operator and viscous terms. Hence, it can be written as

$$RHS_i = - \left[\widehat{C} (Q_i) - \widehat{D} (Q_i) - \widehat{V} (Q_i) \right]. \quad (15)$$

The artificial dissipation operator is computed only in the first two stages for Euler simulation. Therefore, the $(j - 1)'$ superscript in Eq. 14 is equal to 0 in the first time step and equal to 1 in the others. Otherwise, for viscous simulations, the artificial dissipation operator is computed at alternate stages. This approach leads to a low computational cost by stage and guarantees good numerical stability. The α coefficients proposed by Jameson are chosen in the present work. These coefficients are

$$\alpha_1 = \frac{1}{4}, \quad \alpha_2 = \frac{1}{6}, \quad \alpha_3 = \frac{3}{8}, \quad \alpha_4 = \frac{1}{2}, \quad \alpha_5 = 1. \quad (16)$$

This scheme is known as a hybrid scheme because the convective, dissipative and viscous fluxes are not updated in the same stages within a time step.

6. CONVERGENCE ACCELERATION TECHNIQUES

In order to increase convergence ratio of steady simulation three algorithms were used. First of them use a CFL number definition to prescribe to each control volume throughout domain is the higher admissible time step in which convergence is not compromised, and time scales of problem too. Second algorithm is the Implicit Residual Smooth technique. This technique increase convergence ratio acting on residue spreading from i -th control volume to its nb -th neighbours.

These techniques are used in steady and unsteady simulations. As implemented in solver by using Dual-Time-Step algorithm, each unsteady time-step is formed by a set of subsequent steady simulations in which aerodynamic coefficients is not evaluated. Keeping this point in mind, one can conclude that this convergence acceleration techniques is somehow used in unsteady simulations too.

The last algorithm is the know as the unsteady multigrid algorithm and its formulation differs for commonly used one be considering unsteadiness contribution of flow into its formulation, as a source term in residue of inner iterations.

Multigrid schemes sacrifice time accuracy to achieve fast convergence. Using dual-time stepping scheme, the multigrid scheme can be used as a driver to fully implicit time stepping scheme. In this scheme, fast convergence feature of multigrid schemes can be used in unsteady flows simulations.

the fully implicit scheme is an A-stable method for $q=1,2$. In present work $q=2$, was chosen. Work of Jameson(1991) approximates conserved URANS set of equations by:

$$D_t [\nabla^{n+1} \mathbf{Q}^{n+1}] + RHS [\mathbf{Q}^{n+1}] = 0. \quad (17)$$

where next time step is denoted by $n + 1$ notation, hence one can note equation is solved in future information that was not computed yet. Moreover, D_t is a second order backward difference operator:

$$D_t = \frac{1}{\Delta t} \sum_{q=1}^2 \frac{1}{q} [\Delta_-]^q, \quad (18)$$

where,

$$\Delta_- \mathbf{Q}^{n+1} = \mathbf{Q}^{n+1} + \mathbf{Q}^n. \quad (19)$$

If URANS system of equation can be written in a linear differential fashion, such as:

$$\frac{d\mathbf{Q}}{dt} = \alpha \mathbf{Q}, \quad (20)$$

one can applying backward difference operator, Eq. 19, into Eq. 18. Hence, resulting relation is applied into linear differential equation, Eq. 20, resulting following relation in pseudo-time, t^* :

$$\frac{d\mathbf{Q}}{dt^*} - RHS^* (\mathbf{Q}) = 0, \quad (21)$$

where modified residual which is evaluated in pseudo-time steps is defined as:

$$RHS^*(\mathbf{Q}) = RHS(\mathbf{Q}) + \frac{3}{2\Delta t} - \frac{1}{\forall^{n+1}} [S(\mathbf{Q}^n, \mathbf{Q}^{n-1})] . \quad (22)$$

Moreover, the fixed source term due mesh movement is:

$$S(\mathbf{Q}^n, \mathbf{Q}^{n-1}) = \frac{2}{\Delta t} \forall^n \mathbf{Q}^n - \frac{1}{2\Delta t} \forall^{n-1} \mathbf{Q}^{n-1} . \quad (23)$$

For inner iterations, the same explicit RK5 is used to advance solution in modified steady state problem. Hsu and Jameson(2002) improved convergence ratio of inner iteration by using an implicit time-stepping method to advance pseudo-solution in time. This improvement reduces substantially the number of inner iterations.

7. MESH DEFORMATION ALGORITHM

The methodology used in the present work considers the airfoil as a rigid body. However, the physical airfoil is a continuous and flexible body with a infinite number of degrees of freedom (DOFs). The structural model must represent, in a certain way, this natural airfoil flexibility. For the *typical section model*, Bisplinghoff et al.(1955), the airfoil flexibility is represented by two DOFs, *i.e.*, those for airfoil pitching and plunging. These DOFs try to represent a rigid airfoil with the features of a flexible one.

The aerodynamic harmonic external excitation, which is performed as an input for the structural model, induces a harmonically oscillatory response in pitch and plunge to the airfoil. This type of harmonic movement can be seen as a forced motion imposed to the airfoil, in order to study its behaviour in a certain reduced frequency. Actually, the present work has only considered the pitching motion, since its effects are deemed more pronounced for the present applications. Hence, the computational mesh over the airfoil must move accordingly. The mesh moves as a rigid body together with the airfoil. These algorithms require a mesh update at each time step (see Batina et al., 1989 and Raush, 1990 for details). In the present work, once mesh moves rigidly with the airfoil is denoted *rigid mesh case*.

A rigid mesh movement is also considered. In this case, all grid points translate and/or rotate following the harmonic forced airfoil movement. Each grid point has the same type of motion. In this case, the edges are considered totally rigid. The grid points move according to:

$$\begin{aligned} x_i^{n+1} &= (x_0 - x_{EA}) \cos(\alpha(t) - \alpha_0) + y_0 \sin(\alpha(t) - \alpha_0) + \frac{x_{EA}}{2} , \\ y_i^{n+1} &= y_0 + \cos(\alpha(t) - \alpha_0) + (x_0 - x_{EA}) \sin(\alpha(t) - \alpha_0) + h(t) . \end{aligned} \quad (24)$$

In previous equations, α is the DOF for pitching, positive nose up, and h is its pair for plunging, positive to down. For this algorithm, the outer boundary edges move as a rigid body together with all interior grid points. Therefore, there is no relative movement among the nodes. One should observe that the airfoil movement relations always refer to the initial mesh. Such an approach reduces the possibility of cumulative numerical round-off errors for the mesh movement algorithm. These numerical errors are particularly important for turbulent meshes, because the grid is extremely refined near the bodies in order to resolve the turbulence model equations. In order to reduce such type of errors, the aeroelastic viscous code is written using double precision for all cases.

8. RESULTS

8.1 Steady Viscous Results

This section presents viscous results of conventional and supercritical airfoils simulations at transonic regime of flight. These results are incorporated in the work in order to demonstrate high capacity of the solver to predict main structures of turbulent flows.

A simulation over the conventional NACA 64A010 and NACA 0012 airfoils are performed. Both simulations were performed at transonic flow regime in which effects very interest the authors. Figure 2 presents obtained simulated results for the NACA 64A010 airfoil. Results are presented in terms of pressure aerodynamic coefficients on upper surface. A half-C type mesh were used to diminish computational effort due symmetry of the flow. No angle of attack is considered. For this case 60 nodes into boundary layer was considered and $y^+ = 1$. The flighty configuration was at $M_\infty = 0.796$, $Rey = 12$ millions. Results well agree with experimental data of Davis(1992). Moreover, this graphic compares influence of $ak2$ coefficient of artificial dissipation operator on steady results. Results are in well agreement with experimental data of AGARD(1982) . The $ak2$ coefficient influence in viscous simulations is not so determinant to obtain good turbulent results. Its influence is low due large influence of boundary-layer. Boundary layer works to reduce intensity of shock-wave on airfoil surface. In other words, second order derivatives of URANS formulation decrease efficiency of d^2 term near large discontinuity regions. Boundary layer works in viscous flows as an important damping structure to reduce undamping numerical instabilities near large discontinuous regions.

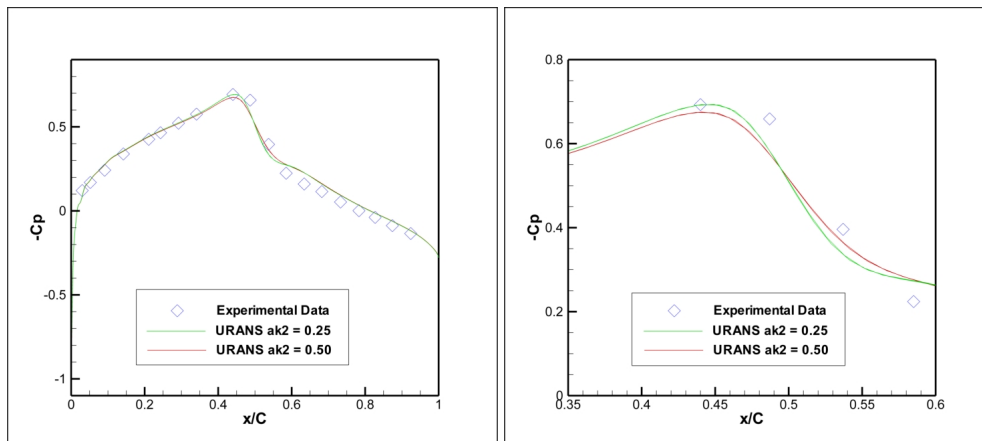


Figure 2. Spalart-Allmaras turbulence model validation, further, $ak2$ coefficient analysis.

The shock-wave characterizes itself by a large discontinuity of flow field variables, such as Mach number, density and pressure, among others. However, using a viscous formulation the shock-wave tends to spread the flow field variables over airfoil surface, hence, less normal the shock-wave is present using viscous formulation. In aerodynamic flows, turbulent boundary layer may detach from airfoil surface causing oscillatory behaviour of math model. It occurs because some simple eddy-viscosity turbulence models are not able to capture such phenomenon. Figure 3 compares, in terms of pressure coefficient distribution for inviscid and viscous formulations. Moreover, convergence histories is also compared for both formulations. Convergence history presents lower convergence ratio of viscous formulation in comparison with

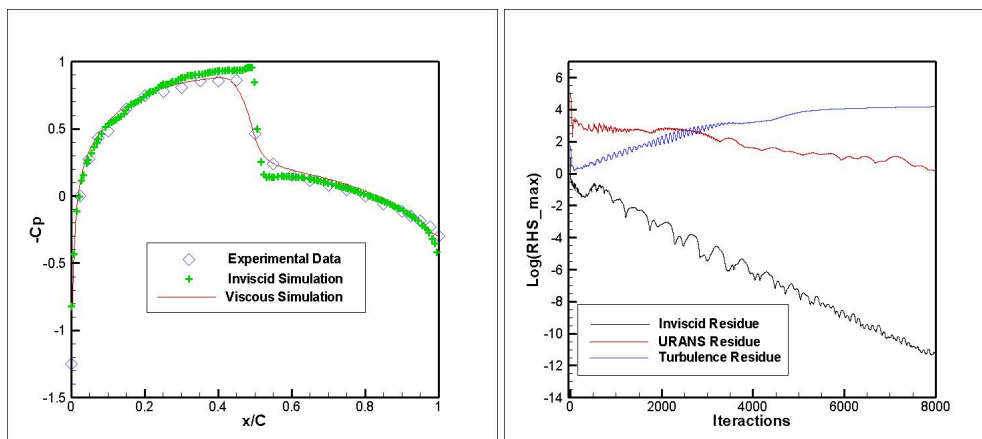


Figure 3. Pressure distribution on a NACA 0012 airfoil surface, inviscid and viscous formulations and convergence histories.

inviscid one. Furthermore, Spalart-Allmaras residue is constant as simulation progress. This behaviour of turbulence model is obtained because turbulence flows need to be constant fed to maintain a certain turbulence model in steady flows. Turbulence model residue does not converge, it tends to maintain constant which suggests a continuous turbulence feed from convective terms of URANS. Results also suggest very well agreement of shock-wave computation using viscous formulation, inviscid formulation over-predicts shock-wave strength due to lack of terms in formulation to capture shock-wave boundary layer interaction. Convergence histories show that inviscid simulation achieves zero machine value.

Moreover, a transonic steady simulation on the OAT 1510 supercritical profile is also performed. In this case one can read the following flow configuration: $M_\infty = 0.724$, $Re_\gamma = 3$ millions and $\alpha_0 = 1.15$ degs. of angle of attack. Figure 4 compares simulated results with experimental data of Rodde and Archambaud (1994). Results show good agreement with experimental data for lower surface and for aft and toward regions of upper surface. However, due to the large simplicity of the turbulence model, the shock-wave position was not well captured. The position was over-predicted using this formulation. In supercritical airfoils, the shock-boundary layer interaction is stronger than conventional airfoils, so a possible boundary layer detachment could be presented and the formulation was not able to well capture it, because this behaviour was not observed in results.

The NLR 7301 airfoil was also simulated in the transonic regime of flight. This is also a supercritical airfoil such as its pair OAT 1510. The NLR airfoil was simulated at Mach number equal to 0.70, with 2 deg. of angle of attack and Reynolds

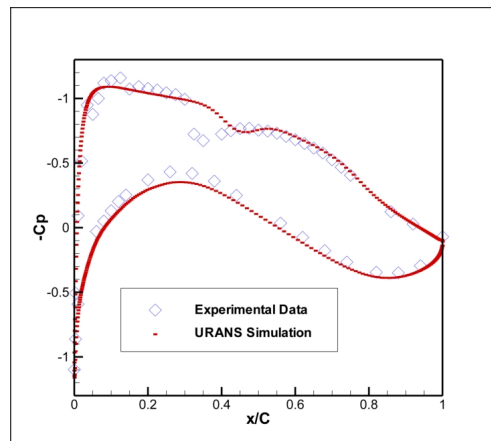


Figure 4. Spalart-Allmaras turbulence model validation on the OAT 1510 supercritical airfoil.

number of 2.14 millions. Experimental data of AGARD(1982) was used to compares inviscid, and viscous results. Once again results were well predicted, except in adjacent regions to shock-wave boundary layer interface. Figure 5 compares simulated results to experimental data. Moreover, as one can observe inviscid formulation over-predicted the shock-wave

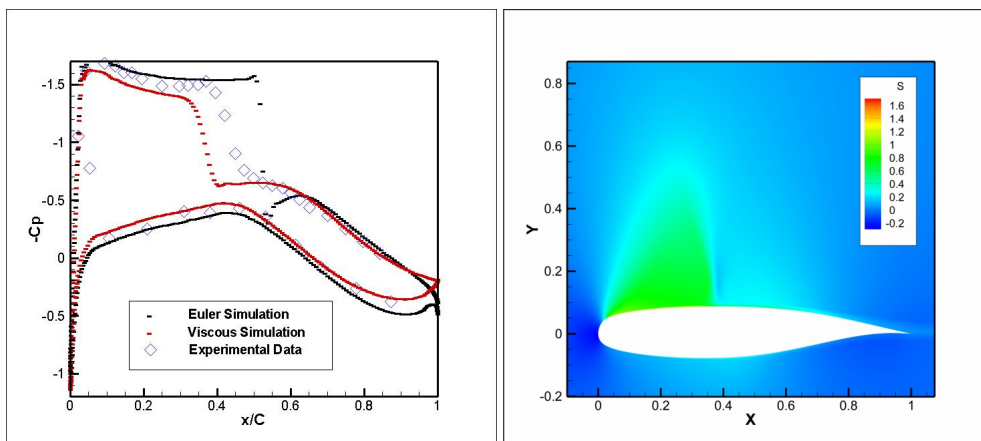


Figure 5. Pressure coefficient and entropy (viscous) distribution on a NLR 7301 supercritical airfoil.

strength, and **no** isentropic recompressibility region is found on upper surface. It is important to analysis once theoretical data of supercritical surface obtain large supersonic isentropic recompressibility region on upper surface. Therefore, shock-wave strength is reduced. Results analysis presents very large entropy generation on airfoil upper surface, compared with viscous data. Entropy gradients are presented into such region on airfoil surface analysing inviscid results. However, for viscous results, except into boundary layer, there are no gradients of entropy generation in such region.

8.2 Unsteady Inviscid Results

In order to start an unsteady simulation, simulation needs start from a steady converged solution for the mean angle of attack of the flow of interest. Steady simulations are considered converged when the lift and moment coefficients stop to change as the iterations progress. It is important to emphasize that the initial steady solutions must be fully converged in order to guarantee good behaviour of unsteady results. Otherwise, unsteady simulation tends to blow up if the convergence of the aerodynamic steady simulations has not been achieved.

The forced motion in the pitch degree of freedom is used as source of external harmonic excitation. This external harmonic force needs a characteristic frequency, known a priori. This frequency is the reduced frequency obtained in relation to the half chord. It is defined as:

$$k = \frac{\omega}{U_\infty} \frac{c}{2}, \quad (25)$$

where c is the airfoil chord, U_∞ is the free stream velocity magnitude, and ω is the frequency of pitch oscillation. Typically, values for the reduced frequency are lower than unity. The prescribed airfoil pitch motion is performed as an increment in

angle of attack over the steady solution. In the present work, the pitch oscillations are performed around the elastic axis. The instantaneous angle of attack can be written as:

$$\alpha = \alpha_0 + \Delta\alpha \sin(\omega t) , \quad (26)$$

where t is the time, α_0 is the initial flow angle of attack and $\Delta\alpha$ is the small pitch oscillation amplitude.

In the present work, the NACA 0012 airfoil is forced to oscillate in pitch with a reduced frequency of 0.0814, mean angle of attack $\alpha_0 = 0.016$ deg., and an oscillation amplitude of 2.51 deg. The elastic axis is located at the quarter-chord point, measured from the leading edge. One of features of present work is to evaluate if Dual-Time-Step technique makes necessary using inviscid formulation. The experimental data was obtained from AGARD(1982). This good agreement happens because the turbulent boundary layer is very thin and the normal shock wave is very strong.

A set of simulations are performed upon the NACA 0012 airfoil at $M_\infty = 0.755$, with, $\alpha_0 = 0.016$ and $\Delta\alpha = 2.51$ degs.. Reduced frequency of pitching oscillation is of 0.0814, based on Eq. 25 formulation. Dual-time stepping method performance is evaluated in terms of hysteresis curves over lift coefficient.

Figure 6 refers to unsteady results of inviscid simulation of NACA 0012 airfoil with no using the Dual-time stepping analysis. At this point, real time step usage is evaluated, only. Results confirm feeling of reducing time steps, simulation shall gets better results than it correspondent higher time step pair. Results are compared in terms of hysteresis curves. These results also suggest that using larger time steps inviscid flows are not able to faster re-adapt itself on airfoil instantaneous angle of attack. This type of simulation uses an unique iteration for each time step. Using this direct formulation results of larger time-steps poor agree with experimental data, and lower time-steps so far. Values suggests reducing real

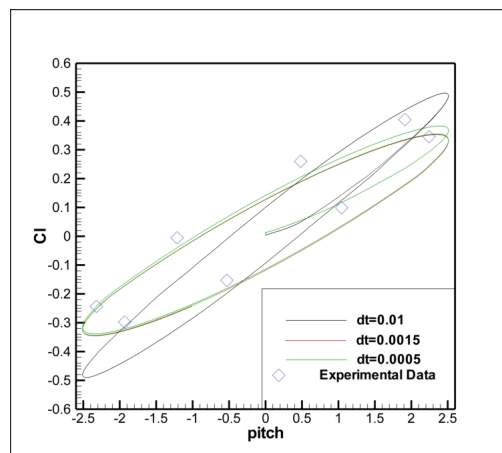


Figure 6. Influence of real time step in lift coefficient hysteresis curves.

time steps of simulations, one can obtain better results, hence first order derivative of conserved URANS vector, $\frac{\partial Q}{\partial t}$, is better represented in a finite volume formulation. As time step tends to zero, continuous, in time, URANS equations is achieved. Results of higher time step, $0.01s$ did not well match with experimental data. It is the black curve in fig. 6. Moreover, curves of $dt = 0.001s$ and $dt = 0.0005s$, red and green respectively, well match each order.

Number of *inner* iterations is an important parameter to evaluate performance of Dual-time stepping, or DTS, method. It parameter refers to number of steady iterations, or inner iterations, to be performed into each real time step of unsteady simulation. As number of inner iterations increases convergence is faster achieved, however, using an explicit time step algorithm large amount of iterations are necessary, such as following steady state simulations.

Following simulations were also performed with same configuration of previously NACA 0012 conventional airfoil. Therefore, the $dt = 0.01s$ was chosen once poor results were obtained without using DTS algorithm. Figure 7 present the aerodynamic coefficients behaviour in time. For lift one, C_l , no larger discrepancies are found. However, for moment coefficient, C_m , larger discrepancies are found at peak of each cycle, as the number of inner steps increase, in other words convergence too, the curve tends to behave more smooth than its pairs with. Higher frequencies errors are eliminated in simulations as number of inner iterations increase.

Figure 8 corroborate the expose previously idea that as number of inner iterations increase airfoil response better match experimental data. This picture compares, in an hysteresis curve fashion for lift coefficient distribution, the influence of the number of inner iterations with experimental data. If number of *inner* iterations is zero, in other words, no using DTS algorithm, hysteresis curve absolutely match curve of 1 *inner* iteration usage. This behaviour is almost expected. It suggests, using an explicit in time discrete finite volume formulation, one iteration does not fast adapted itself to new updated pitch DOF configuration. Moreover, results using 10 and 25 *inner* iterations better match experimental data, exactly as expected by authors.

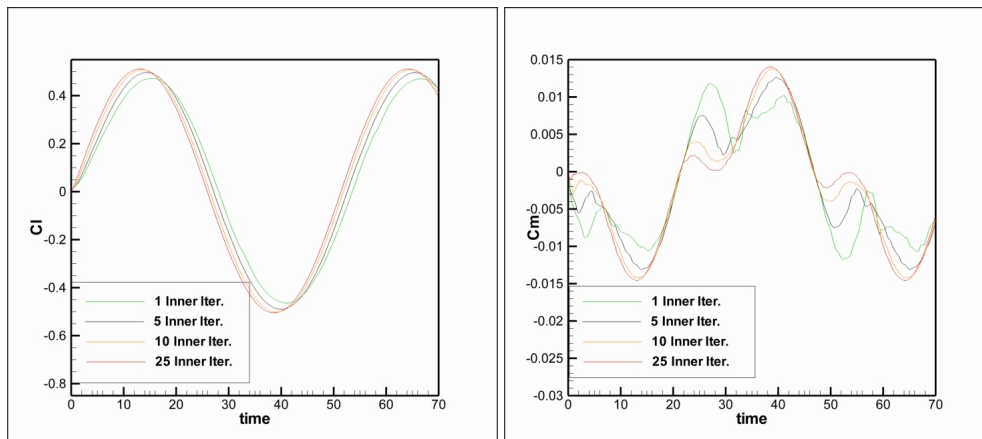


Figure 7. Inner iterations influence on aerodynamic coefficients distribution in time, lift and moment, respectively.

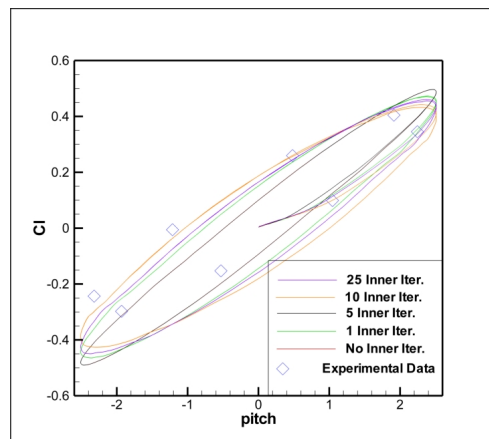


Figure 8. Influence of number of inner interactions in terms of unsteady lift airfoil response.

9. CONCLUSION

The authors prove that using viscous formulation better results are obtained for conventional airfoil than using inviscid formulation. Furthermore, for airfoils simulated in this work, obtained results very well agree with its correspondent experimental data.

Supercritical airfoil results did not very well agree with experimental data. Therefore, turbulent model tries to predict, with moderate success, predict shock-wave boundary layer iteration, but other regions were better captured by viscous formulation than the inviscid one. Moreover, results also presents that turbulent viscous solver is able to receive Dual-Time stepping algorithm to perform flutter analysis. This efforts is expected for future work.

Inviscid unsteady simulations have lead authors to conclude, there is a large dependency of real time step parameter for such flows. But, there is a lower bound in which reducing time step results become constant.

The Dual-Time stepping algorithm demonstrate itself a very powerful method to increase solver accuracy with larger time steps. Using few inner iterations good convergence was obtained for such flows. This behaviour is very proud to occurs due implementation of unsteady multigrid method.

10. ACKNOWLEDGEMENTS

The authors gratefully acknowledge the financial support for this research provided by CAPES (Coordenação de Aperfeiçoamento de Pessoal de Ensino Superior) which provided a MS scholarship to the first author. The authors would also like to acknowledge CNPq, (Conselho Nacional de Desenvolvimento Científico e Tecnológico) which partially supported the project under the Research Grant No. 312064/2006-3.

11. REFERENCES

AGARD, 1982, Various Authors, "Compendium of Unsteady Aerodynamic Measurements", AGARD-R-702.

- Batina J. T., 1989, "Unsteady Euler Airfoil Solutions Using Unstructured Dynamic Meshes," *27th AIAA Aerospace Sciences Meeting*, AIAA Paper No. 89-0115, Reno, NV.
- Batina J. T., 1991, "Unstructured Grid Methods Development - Lessons Learned," *Proceedings of the 4th International Symposium on Computational Fluid Dynamics*, Vol. I, Davis, CA.
- Bigarella, Enda Dimitri V. and Azevedo, J.L.F., 2007, "Advanced Eddy-Viscosity and Reynolds-Stress Turbulence Model Simulations of Aerospace Applications," *AIAA Journal*, Vol. 45, No. 10, pp. 2369–2390.
- Bisplinghoff, H. L., Ashley, H., Halfman, R. L., 1955, *Aeroelasticity*, dison-Wesley, Reading, Mass.
- Darracq, D., Champagneux, S., Corjon, A., 1998, "Computation of Unsteady Turbulent Airfoil Flows with an Aeroelastic AUSM+ Implicit Solver," *AIAA Paper*, AIAA-98-2411.
- Davis, S., 1982, "NACA 64A010 Oscillatory Pitching, Compendium of Unsteady Aerodynamic Measurements," AGARD-R-702.
- Hsu, J.M., and Jameson, A., 2002, "An Implicit-Explicit Hybrid Scheme for Calculating Complex Unsteady Flows", AIAA paper 2002-0714, *40th AIAA Aerospace Sciences Meeting and Exhibit, Reno, Nevada*, January, 14-17.
- Jameson A., Schmidt, W. and Turkel, E., 1981, "Numerical Solution of Euler Equations by finite Volume Methods Using Runge-Kutta Time Stepping Schemes," *AIAA 14th Fluid and Plasma Dynamics Conference*, AIAA Paper 81-1259, Palo Alto, CA.
- Jameson, A., and Mavriplis, D., 1986, "Finite Volume Solution of the Two-Dimensional Euler Equations on a Regular Triangular Mesh", *AIAA Journal*, Vol. 24, No. 4, pp. 611-618.
- Jameson, A., and Baker, T.J., 1987, "Improvements to the Aircraft Euler Method", AIAA Paper 89-0115, *25th Aerospace Sciences Meeting*, Reno, NV.
- Jameson, A., 1991, "Time Dependent Calculations Using Multigrid, with Applications to Unsteady Flows Past Airfoils and Wings", AIAA paper 91-1596, *10th Computational Fluid Dynamics Conference*, Honolulu, HI, June, 24-16.
- Jameson, A., 1991, "Time Dependent Calculations Using Multigrid, with Applications to Unsteady Flows Past Airfoils and Wings", AIAA 91-1596.
- Lisandrin, P., Carpentieri G., and van Tooren, M., 1986, "Investigation over CFD-Based Models for the Identification of Nonlinear Unsteady Aerodynamics Responses" *AIAA Journal*, Vol. 44, No. 9, pp. 2043–2050.
- Marques A.N., 2004, "Aerospace Simulations of Unsteady Flows Using Unstructured Meshes," Under-Graduation Project, Instituto Tecnológico de Aeronáutica, São José dos Campos, SP, Brazil.
- Marques A.N., 2007, "A Unified Discrete-Time Approach to the State Space Representation of Aeroelastic Systems," Graduation Thesis, Instituto Tecnológico de Aeronáutica, São José dos Campos, SP, Brazil.
- Mavriplis, D.J., 1990, "Accurate Multigrid Solution of the Euler Equations on Unstructured and Adaptive Meshes," *AIAA Journal*, Vol. 28, No. 2, pp. 213–221.
- Nadarajah, S.N., and Jameson, A., 2007, "Optimum Shape Design for Unsteady Flows with Time-Accurate Continuous and Discrete Adjoint Methods" *AIAA Journal*, Vol. 45, No. 7, pp. 1478–1491.
- Oliveira L.C., 1993, "A Aeroelastic State Space Analysis Using Aerodynamics Computational Techniques," *Master Thesis, in portuguese, Instituto Tecnológico de Aeronáutica*, São José dos Campos, SP, Brazil.
- Raush, R.D., Batina, J.T. and Yang H.T., 1990, "Euler Flutter Analysis of Airfoil Using Unstructured Dynamic Meshes," *Journal of Aircraft*, Vol. 27, No. 5, pp. 436–443.
- Raveh, D.E., 2008, "A Numerical Study of an Oscillating Airfoil in Transonic Flows With Large Shock Wave Oscillations," *49th AIAA/ASME/ASCE/AHS/ASC Structures, Structural Dynamics, and Materials Conference Paper No. 2008-1756*, Schaumburg, IL, pp. 1–19.
- Simões C.F.C. and Azevedo J.L.F., 1999, "Unsteady Airfoil Inviscid Flow Simulations Using Unstructured Dynamic Meshes," *Anais do 15th Congresso Brasileiro de Engenharia Mecânica*, Bauru, SP, Brazil.
- Spalart, S.A. and Almaras, S.R., 1994, "A One-Equation Turbulence Model for Aerodynamic Flows," *La Recherche Aérospatiale*, No. 1, pp. 5–21.
- Strauss, D. and Azevedo, J.L.F., 1999, "A Numerical Study of Turbulent Afterbody Flows Including a Propulsive Jet," *Proceedings of the 17th AIAA Applied Aerodynamics Conference*, AIAA Paper No. 99-3190, Norfolk, VA, pp. 654–664.
- Swanson, R.C., Radespiel R. and Turkel E., 1997, "Comparison of Several Dissipation Algorithms for Central Difference Schemes," *AIAA Paper*, No. 97-1945, pp. 580–598.
- Swanson, R.C. and Radespiel R., 1991, "Cell Centered and Cell Vertex Multigrid Schemes for the Navier-Stokes Equations," *AIAA Journal*, Vol. 29, No. 5, pp. 697–703.
- Rodde, A.M., and Archambaud, J.P., 1994, "OAT 15A Airfoil Data, A Selection of Experimental Test Cases for the Validation of CFD Codes", NATO, AGARD-AR-303, Case 11.

12. Responsibility notice

The authors are the only responsible for the printed material included in this paper.